$Ni_{24.7}Ti_{50.3}Pd_{25.0}$ high temperature shape memory alloy with narrow thermal hysteresis and high thermal stability

K.V. Ramaiah*[,a], C.N. Saikrishna[a], Gouthama[b], S.K. Bhaumik[a]

[a]Materials Science Division, CSIR-National Aerospace Laboratories, Bangalore 560 017, India
[b]Department of Materials Science and Engineering, Indian Institute of Technology, Kanpur 208 016, India

Abstract

High temperature shape memory alloys with operating temperatures above 100°C are in demand for use as solid-state thermal actuators in aerospace, automobile and other engineering applications. The present study deals with transformation behaviour and thermal stability of $Ni_{24.7}Ti_{50.3}Pd_{25.0}$ (at.%) high temperature shape memory alloy, in cast and homogenized condition. The martensite finish temperature and transformation hysteresis of the alloy were determined to be 181.0°C and ~8.5°C respectively. The alloy showed high stability upon stress-free thermal cycling, variation in transformation temperatures being ±1°C. The narrow thermal hysteresis and high thermal stability of the alloy upon transformation cycling has been discussed and correlated with its microstructural features, activation energy and elastic strain energy of thermoelastic martensitic transformation. The alloy exhibited modulus of ~82 GPa and hardness of ~4.7 GPa in martensite phase.

Keywords: Shape memory alloy; NiTiPd; Thermal cycling; Thermal hysteresis; Microstructure; Transmission electron microscopy

1.0 Introduction

Among various shape memory alloys (SMAs), near equi-atomic NiTi alloys are the most commercially successful ones [1-2]. The operating temperatures of these alloys, however, are limited to a maximum of about 100°C. Many applications in aerospace, automobile, chemical, power plant and other engineering fields require high temperature shape memory alloys (HTSMAs) which can operate at temperatures >100°C for design of solid-state thermal actuators [3-4]. The applications wherein high actuation/response frequency is the primary requirement, thermal hysteresis of SMAs is of great concern. Lower the thermal hysteresis faster is the actuator response.

Addition of ternary alloying elements such as Pd, Pt, and Au replacing Ni, and Hf, Zr replacing Ti are known to increase the transformation temperatures (TTs) in NiTi alloys [5-7]. While the transformation hysteresis of NiTi-Pt/Au alloys are reported to be comparable to that of binary NiTi alloys (25-40°C) [3,8], addition of Hf/Zr widens the hysteresis to 35-70°C [6,9]. Palladium addition to NiTi alloys, however, are shown to narrow the transformation hysteresis, in the range 15-25°C [10]. Hence, for thermal actuator applications in the

*Corresponding author. Tel: +91 80 25086282; fax: +91 80 25270097. Email address: kvramaiah@nal.res.in

temperature range 100-200°C, NiTiPd HTSMA is a potential alloy system and has received significant attention for further research.

Studies by Cui *et al.* [11] and Zarnetta *et al.* [12] have shown that hysteresis in SMAs is low when the lattice geometric compatibility between transforming phases is high. It has been shown [9,11,12] that in NiTiX (X=Pd, Pt, Au, Cu) alloy systems, minimum hysteresis is reached when the compatibility condition approaches λ_2=1, where λ_2 is the middle eigenvalue of the transformation matrix. Mathematically, λ_2 is defined as $b/\sqrt{2}.a_0$, where a_0 and b are the lattice constants in cubic austenite and orthorhombic martensite phase respectively. Subsequent study by Delville [13] on NiTiPd alloys with varying compositions showed that when λ_2 approaches 1, microstructure of the alloy changes from a lamellar morphology of fully twinned martensite to a morphology of twinless martensite. The same study, further showed that an alloy of composition $Ni_{40}Ti_{50}Pd_{10}$ (at.%) has a low thermal hysteresis of 12°C. However, the TTs of this alloy was significantly low (M_f:~13°C) and hence, it does not fall under the category of HTSMA. In the present study, a NiTiPd HTSMA with M_f of ~180°C and transformation hysteresis of ~8.5°C is being reported. The thermal stability of the alloy upon transformation cycling is discussed and correlated with its microstructural features, activation energy and elastic strain energy of thermoelastic martensitic transformation.

2.0 Experimental procedure

Alloy of nominal composition $Ni_{24.7}Ti_{50.3}Pd_{25.0}$ (at.%) was prepared using high purity titanium (99.97%), nickel (99.99%) and palladium (99.99%) by non-consumable vacuum arc melting process. The cast button was re-melted five times to ensure melt homogeneity. Homogenization of the cast alloy was carried out at 1050°C for 24 h in argon atmosphere, followed by furnace cooling. The TTs of the alloy were determined using differential scanning calorimeter (DSC), TA Instruments - Q2000, as per ASTM-F2004 standard. The DSC scans were carried out at a heating/cooling rate of 10°C/min using nitrogen as purge gas. The effect of heating rate on TTs was studied by varying the heating/cooling rate in the range 2-30°C/min. Transmission electron microscopy (TEM) was carried out using FEI-Tecnai G^2 U-Twin microscope operating at 200 kV. TEM thin foil specimens of homogenized alloy were prepared by mechanical polishing to ~100 μm thickness, followed by sectioning of 3 mm diameter disks using spark-erosion process. Electron transparent regions were obtained by twin jet electro-polishing of disks using an electrolyte mixture of 20 vol.% H_2SO_4 and 80 vol.% methanol at -10°C. Mechanical properties were studied by using CSM NHT S/N:04-00114 instrumented nanohardness tester. Berkovich diamond indenter B-L72, with loads of 10, 50, 100, 150 and 200 mN was used for hardness measurements. Measurements were carried out at different locations with incremental loads at room temperature (25°C). The indentation hardness (H_{IT}) and modulus (E_{IT}) were calculated from initial slope of the unloading curve using Oliver and Pharr method [14].

3.0 Results

Figure 1 shows transformation behaviour of homogenized $Ni_{24.7}Ti_{50.3}Pd_{25.0}$ alloy upon stress-free thermal cycling. The characteristic transformation temperatures of martensite start (M_s), peak (M_p), finish (M_f) and austenite start (A_s), peak (A_p), finish (A_f) temperatures determined from DSC scans using tangent method are reported in Table 1. Results show that the alloy has a single-step phase transformation during heating as well as cooling cycle. The high and low temperature phase of the alloy has been identified [13,15] to be of B2 cubic and B19 orthorhombic structure, respectively. The M_f and A_f were determined to be 181.0 and 201.9°C respectively (Table 1). The transformation hysteresis of the alloy, A_f-M_s, was measured to be ~8.5°C. The hysteresis observed in the present alloy (~8.5°C) is significantly low compared to that reported in literature [16] (~15.7°C) for NiTiPd alloys with similar Pd contents.

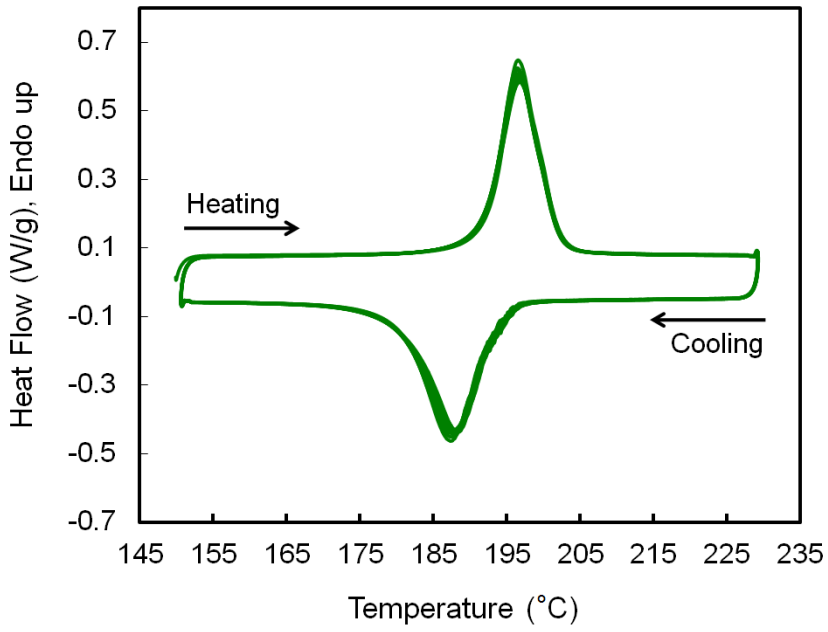

Figure 1 DSC plot shows stress-free thermal cycling behaviour of $Ni_{24.7}Ti_{50.3}Pd_{25.0}$ alloy.

Table 1 Transformation temperatures, and ΔH for heating/cooling of homogenized $Ni_{24.7}Ti_{50.3}Pd_{25.0}$ alloy

Thermal Cycle #	Transformation Temperatures (°C)						ΔH^{a-m} (J/g)	ΔH^{m-a} (J/g)	Hysteresis (A_f-M_s)	Calculated	
	M_f	M_p	M_s	A_s	A_p	A_f				$\Delta E_{el.s.e}^{a-m}$ (J/g)	ΔE_f^{a-m} (J/g)
Cycle.2	181.0	187.6	192.4	191.8	195.9	201.9	21.61	21.44	8.5	0.028	0.19
Cycle.12	181.6	188.9	193.5	191.8	196.3	202.0	21.38	21.36	8.5	0.025	0.17
Cycle.35	182.7	189.0	192.7	192.7	196.5	200.3	21.29	21.25	7.6	0.007	0.17

Results of repetitive phase transformation cycling carried out using DSC (Fig.1) indicate that transformation behaviour of the alloy upon thermal cycling is highly stable. After 35 cycles of heating and cooling, the DSC scans were found to overlap. The TTs and enthalpy of the alloy varied by ±1°C and ±0.2 J/g respectively (Table 1, Fig.1). In general, instability in transformation behaviour arises from thermodynamic contributions of elastic strain energy and frictional work [17,18]. Thermodynamically, the driving force for phase transformation is the energy balance between Gibb's free energy of austenite and martensite phases. The Gibb's free energy change during thermoelastic martensitic transformation consists of chemical and non-chemical energies. The chemical energy is reversible in nature and depends on crystal structure of the phases. The non-chemical energy consists of two components: (a) elastic strain energy and (b) energy dissipation due to frictional work. Elastic strain energy is associated with elastic accommodation of crystallographic volume and shape changes that take place during phase transformation. On the other hand, energy dissipation due to frictional work arises because of the resisting force acting on the moving interfaces during interaction with frictional barriers such as defects, twin/phase boundaries, grain boundaries, second phase particles. In general, low stored elastic strain energy indicates better crystallographic compatibility between the transforming phases. For the present alloy, elastic strain energy and frictional work were estimated using the following thermodynamic equations [17,18].

$$\Delta E_{el.s.e} = \Delta S \{(M_s - T_0) - \Delta E_f^{a-m}\} \quad (1)$$

$$\Delta E_f^{a-m} = \Delta S \{(M_p - A_p)/2)\} \quad (2)$$

$$\Delta S = (-\Delta H^{a-m}/T_0);\ T_0 = (M_s + A_f)/2 \quad (3)$$

where ΔS is the change in chemical entropy (J/g.K), T_0 the equilibrium transformation temperature (K), $\Delta E_{el.s.e}$ the reversible elastic strain energy change (J/g), ΔH^{a-m} the enthalpy of transformation (J/g), and ΔE_f^{a-m} the frictional work (J/g) from austenite to martensite.

The values of TTs and ΔH^{a-m} were obtained from DSC scans (Table 1). From these measured values, the $\Delta E_{el.s.e}$ was calculated using equations (1) to (3). The estimated value for ΔE_f^{a-m} was found to be in the range 0.17 to 0.19 J/g (Table 1**)**. The $\Delta E_{el.s.e}$ was calculated to be in the range 0.007 to 0.028 J/g (Table 1). This elastic strain energy is significantly low compared to 0.35-1.2 J/g for binary NiTi alloy in fully annealed condition [17,18].

Figure 2a shows the effect of heating rate (2 to 30°C/min) on transformation behaviour of $Ni_{24.7}Ti_{50.3}Pd_{25.0}$ alloy. The TTs, and ΔH for heating/cooling cycles are given in Table 2. Results indicate that heating rate has minor influence on A_s and M_s, the variation being within 1°C. In comparison, the heating rate dependence of M_f and A_f was more, the former decreased by ~2°C and the latter increased by ~4°C. The ΔH values remained almost constant and were in the range 21.22 to 21.52 J/g. Transformation hysteresis of the alloy increased monotonically from 5.9 to 9.4°C with increase in heating rate (Table 2). This trend in variation of TTs and the

transformation hysteresis is in accordance with the findings of Wang *et al* [19], wherein it has been shown that increase in heating rate results in larger variation of M_f/A_f than A_s/M_s, and hysteresis. However, the magnitude of variation in TTs and hysteresis in the present alloy is lower than the reported values of 6-10°C in NiTi-base alloys [19,20].

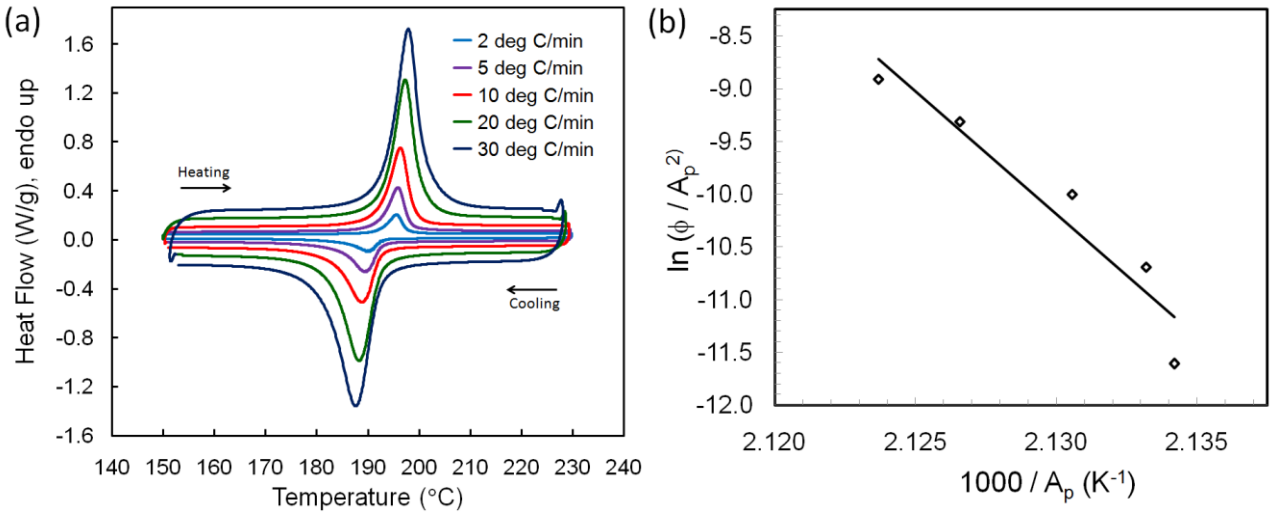

Figure 2 (a) DSC plots of $Ni_{24.7}Ti_{50.3}Pd_{25.0}$ alloy at different heating rates (b) plot of $\ln(\phi/A_p^2)$ vs. $1/A_p$ showing activation energy fitting curve using Kissinger method.

Table 2 Transformation behaviour of homogenized $Ni_{24.7}Ti_{50.3}Pd_{25.0}$ at different heating rates

Heating rate, ϕ	Transformation Temperatures (°C)						ΔH^{a-m} (J/g)	ΔH^{m-a} (J/g)	Hysteresis (A_f-M_s)
(°C/min)	M_f	M_p	M_s	A_s	A_p	A_f			
2	182.2	189.7	192.0	192.2	195.6	197.9	21.52	21.37	5.9
5	183.6	189.5	192.4	192.1	195.8	198.7	21.38	21.34	6.6
10	182.7	189.0	192.6	192.1	196.4	200.2	21.36	21.31	7.6
20	181.9	188.3	192.6	192.9	197.2	200.9	21.35	21.32	8.3
30	180.6	187.7	192.5	192.9	197.9	201.9	21.25	21.22	9.4

The activation energy of phase transformation for the alloy was estimated using the relation proposed by Kissinger [21] for study of solid-state phase transition kinetics. According to Kissinger, irrespective of reaction order, activation energy (E_a) can be calculated from the change in peak transformation temperature brought out by the change in heating or cooling rate and is given by equation (4).

$$d\{\ln(\phi/A_p^2)\}/d(1/A_p)=(-E_a/R) \quad (4)$$

where, the terms ϕ, A_p and R are the heating rate used for DSC experiment, peak temperature of martensite to austenite transformation in Kelvin (K) and universal gas constant (8.314 kJ/mol.K), respectively. The slope of the plot $\ln(\phi/A_p^2)$ vs. $1/A_p$ gives the value of $-E_a/R$.

Figure 2b shows the plot of $\ln(\phi/A_p^2)$ vs. $1/A_p$ drawn using the data provided in Table 2. The calculated E_a, 1931 kJ/mol, for the present alloy is significantly higher than that for Cu-Zn-Al (350-450 kJ/mol) and Ni-Ti (210-531 kJ/mol) shape memory alloys [22-24].

Results of TEM study on $Ni_{24.7}Ti_{50.3}Pd_{25.0}$ alloy are presented in Fig.3. The study revealed three distinct features in the microstructure of alloy, which includes (i) martensite plates with varying twin width ratio, (ii) domains with anti-phase boundaries like (APB-like) structure, and (iii) regions of twinless martensite. Twin width ratio is defined as the ratio of width of two martensite plates accommodating a habit plane with austenite ('a/b' indicated in Fig.3a). The martensite plates in the microstructure consist of variable twin width ratio, the majority being small twin width ratio type (Fig.3a) [25]. The APB-like structure can be seen in Fig.3b. The selected area electron diffraction (SAED) patterns corresponding to Fig.3a and 3b are shown in Fig.3c and 3d respectively. The SAED pattern analysis conforms to B19 structure. Regions of twinless martensite are shown in Fig.3e. The microstructure of the alloy also shows high degree of atomic order on either side of martensite plates with sharp twin boundary (Fig.3f). Figure 3f is the high resolution image wherein the Inverse Fast Fourier Transform (IFFT) is added to experimental image for contrast enhancement. Figure 3g illustrates the FFT obtained from experimental image and the diffraction spots have been indexed on simulated SAED pattern. The SAED pattern was found to conform to B19 structure.

The deformation behaviour of $Ni_{24.7}Ti_{50.3}Pd_{25.0}$ alloy in martensite phase (at 25°C) was studied using nanoindentation method. Indentation hardness (H_{IT}) and modulus (E_{IT}) were calculated based on the method suggested by Oliver and Pharr [14]. The results obtained are given in Table 3. The average values of H_{IT} and E_{IT} were about 4.7 GPa and 82 GPa respectively. These values were found comparable to that reported [26-28] for binary Ni-Ti alloys. Figure 4 shows the load vs. penetration depth curves at different locations on the sample with incremental loads. It can be seen that the slopes of loading curves with incremental loads overlapped each other. This continuous nature of loading curves without any sink-in or pop-in is indicative of absence of shear bands underneath indentation [29]. This implies that deformation in the material is by pure detwinning and reorientation of martensite variants [30], an indication of ease of movement of twin boundaries/interfaces in the microstructure. Also, since various deformation mechanisms are active during the indentation process, the modulus values reported in this study are apparent Young's modulus and not true Young's modulus.

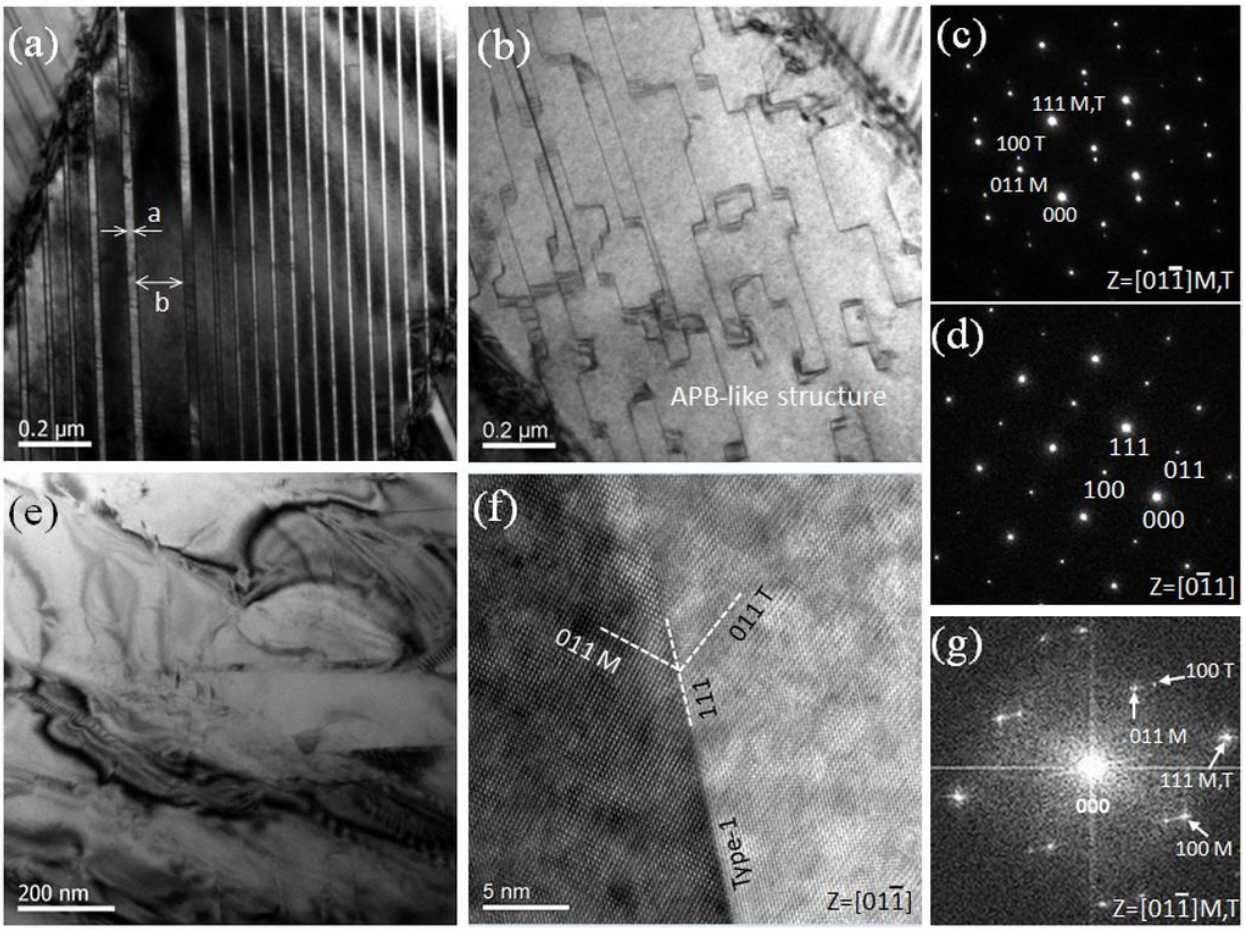

Figure 3 TEM images and electron diffraction patterns of $Ni_{24.7}Ti_{50.3}Pd_{25.0}$ alloy: (a) Bright field image showing small twin width ratio martensite (twin width ratio: 'a/b'); (b) APB-like structures with linear and curved/angular loops; (c) and (d) SAED patterns of (a) and (b), respectively; (e) Illustration of a twinless martensite; (f) High resolution image of martensite variants with sharp twin boundary, experimental image added with Inverse Fast Fourier Transform-IFFT image for contrast enhancement; and (g) corresponding FFT obtained from experimental image and the diffraction spots indexed on simulated SAED pattern.

Table 3 Indentation hardness (H_{IT}) and Indentation modulus (E_{IT}) of $Ni_{24.7}Ti_{50.3}Pd_{25.0}$ alloy

Property[$]	Applied load (mN)				
	10	50	100	150	200
H_{IT} (GPa)	4.7 ± 0.5	4.6 ± 0.7	4.9 ± 0.1	4.5 ± 0.3	4.6 ± 0.1
E_{IT} (GPa)	81 ± 7.8	85 ± 4.2	79 ± 3.3	81 ± 3.3	82 ± 1.6
Depth at maximum load (nm)	389 ± 18.9	911 ± 8.2	1282 ± 16.4	1625 ± 40	1852 ± 22

[$]mean value of 3 indents at each load with ± standard deviation

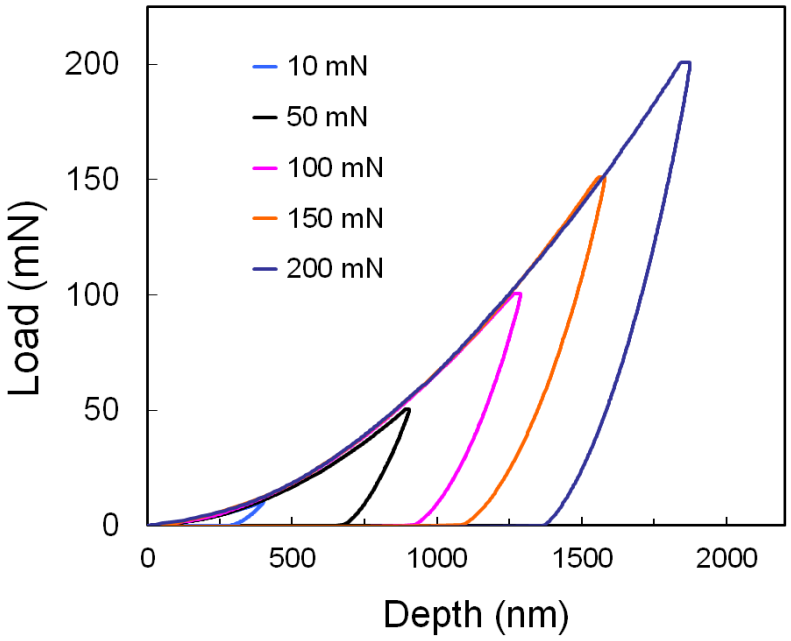

Figure 4 Load vs. penetration depth in $Ni_{24.7}Ti_{50.3}Pd_{25.0}$ alloy during loading-unloading at different locations determined using nanoindentation method.

4.0 Discussion

Experimental results show that $Ni_{24.7}Ti_{50.3}Pd_{25.0}$ HTSMA has high thermal stability upon thermal cycling (Fig.1) and it shows marginal shift in TTs at different heating rates (Fig.2a). Also, thermal hysteresis of the alloy was found to be relatively low (8.5°C). Hysteresis during phase transformation arises because of dissipation of input energy as frictional work and/or heat. For an alloy to be thermally stable, the dissipation of input energy must be minimal. The narrow hysteresis observed in the present alloy clearly indicates that the irreversible energies associated with phase transformation are significantly low. The irreversible energy is essentially the combination of frictional energy loss and plastic deformation during phase transformation [17,31,32]. The energy loss is due to friction associated with movement of twin interfaces, phase/twin boundaries, etc. Studies [33-35] have shown that the lattice internal friction is highest at M_s and is associated with nature of microstructure of martensite phase. On the other hand, plastic deformation often occurs in shape memory alloys due to strain constraint at the interfaces as a consequence of transformation shear and associated volume change during phase transformation. The low frictional work of 0.17-0.19 J/g estimated using thermodynamic relations for the present alloy, compared to ~1.0 J/g for Ni-Ti alloy [17], further ascertains the low irreversible energy of phase transformation.

Activation energy of alloy provides an insight into the nucleation and growth kinetics of thermoelastic martensite phase transformation. In general, high activation energy of solid-state phase transformation signifies

highly cooperative movement of atoms/interfaces in the microstructure [22,24,36]. This cooperative movement of atoms is favored when the crystal lattice in alloy has highly ordered structure with minimal vacancies/defects. Also, the magnitude of activation energy, though dependent on alloy composition, in a particular alloy system, it indicates the atomic ordering of the transforming phases [24]. Higher the activation energy better is the atomic ordering. In contrast, an alloy with low activation energy [22] signifies vacancies/defects/disorder in the crystal lattice and therefore, the movement of atoms to their equilibrium positions during phase transformation becomes relatively easy. The high activation energy (1931 kJ/mol) estimated for the present alloy indicates high degree of atomic order in the crystal lattice, thereby resulting in a stable behaviour upon thermal cycling. The high degree of ordering in martensite phase is also confirmed by high resolution TEM image shown in Fig.3f.

The microstructure of $Ni_{24.7}Ti_{50.3}Pd_{25.0}$ alloy showed distinctive features such as regions of twinless martensite, small twin width ratio martensite and APB-like structures (Fig.3). These microstructural features are the result of lattice geometric compatibility (λ_2) between the transforming phases [13,25]. Study by Grossmann *et al* [36] has shown that the transformation thermal hysteresis and cyclic stability in SMAs are related to crystallographic compatibility. Narrow thermal hysteresis and improved functional fatigue properties were observed when λ_2 approaches 1, i.e., the crystallographic misfit between austenite and martensite phase is small. This in turn results in low elastic strain energy at the interfaces and narrow thermal hysteresis. The lower elastic strain energy (0.007-0.028 J/g), narrow thermal hysteresis (8.5°C) and the microstructural features observed in the present study of NiTiPd alloy indicates small crystallographic misfit between the transforming phases. Presence of APB-like structure has also been reported in Ti-Pd and Ti-Ni-Pd SMAs [13,37,38]. It has been established [37,38] that these APB-like structures are different from the classic APB defects that form during order-disorder transformation and have ribbon-like appearance with linear as well as angular/curved contrast (Fig.3b). Since interfaces of APB-like structures are unlike APB defects, they offer relatively less resistance to transforming/moving interfaces, thereby lowering the transformation hysteresis. Studies [11-13,39] have shown that when the transforming phases are geometrically compatible, no lattice invariant shear is required for habit plane to exist during transformation and hence, the formation of twinless martensite (Fig.3e). The existence of twinless martensite also explains the low elastic strain energy of phase transformation (0.007-0.028 J/g) observed in the alloy. The elastic strain energy arises because of the accommodation of transformation shear and associated volume change that takes place during phase transformation. As the number of interfaces is reduced, the contribution of interfacial energy towards elastic strain energy decreases, thereby resulting in lower values. These distinct microstructural features observed in the alloy are in turn responsible for its low hysteresis of phase transformation and high thermal stability.

5.0 Conclusions

The transformation behaviour and thermal stability of $Ni_{24.7}Ti_{50.3}Pd_{25.0}$ (at.%) high temperature shape memory alloy, in homogenized condition was studied. The alloy showed a high martensite finish temperature of 181.0°C and therefore is potential candidate material for design of high temperature solid-state thermal actuators. The following major conclusions can be drawn from the study.

(1) $Ni_{24.7}Ti_{50.3}Pd_{25.0}$ alloy showed narrow transformation hysteresis of ~8.5°C. The stability of the alloy upon stress-free thermal cycling is also high, variation in transformation temperatures being ±1°C.

(2) High activation energy of 1931 kJ/mol and low elastic strain energy of 0.028 J/g during austenite-martensite phase transformation is found to be the reasons for narrow thermal hysteresis and high thermal stability.

(3) The distinct microstructural features such as regions of twinless martensite, low twin width ratio martensite, and APB-like structures have significant effect in lowering of thermal hysteresis of the alloy and thereby, imparting thermal stability upon transformation cycling.

(4) The alloy exhibited modulus of ~82 GPa and hardness of ~4.7 GPa in martensite phase.

Acknowledgements

The work presented in this paper was carried out with the financial support under National Programme on Micro and Smart Systems (NPMaSS, PARC#1:3), Aeronautical Development Agency (ADA), DRDO, Bangalore, India. The help received from Dr. Harish Barshilia for nanoindentation and Mr. J. Bhagyaraj for TEM work is gratefully acknowledged.

References

[1] Melton KN. Ni-Ti based shape memory alloys. In: Duerig TW, Melton KN, Stockel D, Wayman CM, editors. Engineering aspects of shape memory alloys, London, Butterworth- Heinemann; 1990, p. 21-35.

[2] Huang W. On the selection of shape memory alloys for actuators. Mater Des 2002; 23: 11-9.

[3] Ma J, Karaman I, Noebe RD. High temperature shape memory alloys. Inter Mater Rev 2010; 55:304-15.

[4] Quackenbush T, MckillipJr R. Selected applications of aeropropulsion actuation and shape control devices using HTSMAs. Metall Mater Trans A 2012; 43:2870-81.

[5] Donkersloot HC, Van Vucht JHN. Martensitic transformations in gold-titanium palladium-titanium, and platinum-titanium alloys near the equiatomic composition. J Less-Common Met 1970; 20:83-91.

[6] AbuJudom II DN, Thoma PE, Kao M, Angst DR. High transformation shape memory alloy. US Patent No. 5,114,504, 1992.

[7] Eckelmeyer KH. The effect of alloying on the shape memory phenomenon in Nitinol. Scripta Metall 1976; 10:667-72.

[8] Lindquist PG, Wayman CM. Shape memory and transformation behaviour of martensitic Ti-Pd-Ni and Ti-Pt-Ni alloys. In: Duerig TW, Melton KN, Stockel D, Wayman CM, editors. Engineering aspects of shape memory alloys, London: Butterworth-Heinemann; 1990, p. 58-68.

[9] Zhang Z, James RD, Muller S. Energy barriers and hysteresis in martensitic phase transformations. Acta Mater 2009; 57:4332-52.

[10] Bigelow G, Padula-II S, Garg A, Gaydosh D, Noebe R. Characterization of ternary NiTiPd high-temperature shape-memory alloys under load-biased thermal cycling. Metall Mater Trans A 2010; 41:3065-79.

[11] Cui J, Chu YS, Famodu OO, Furuya Y, Hattrick-Simpers J, James RD, et al. Combinatorial search of thermoelastic shape-memory alloys with extremely small hysteresis width. Nat Mater 2006; 5:286-90.

[12] Zarnetta R, Takahashi R, Young ML, Savan A, Furuya Y, Thienhaus S, et al. Identification of quaternary shape memory alloys with near-zero thermal hysteresis and unprecedented functional stability. Adv Funct Mater 2010; 20:1917-23.

[13] Delville R. From functional properties to micro/nano-structures: a TEM study of TiNi(X) shape memory alloys. PhD Thesis, University of Antwerp, Germany, 2010.

[14] Oliver WC, Pharr GM. An improved technique for determining hardness and elastic modulus using load and displacement sensing indentation experiments. J Mater Res. 1992; 7:1564-83.

[15] Ramaiah KV, Saikrishna CN, Gouthama, Bhaumik SK. Microstructure and transformation behaviour of $Ni_{75-X}Ti_XPd_{25}$ high temperature shape memory alloys. J Alloys Compd 2013; 554:319-26.

[16] Atli KC, Karaman I, Noebe RD, Garg A, Chumlyakov YI, Kireeva IV. Improvement in the shape memory response of $Ti_{50.5}Ni_{24.5}Pd_{25}$ high-temperature shape memory alloy with Scandium micro-alloying. Metall Trans A 2010; 41:2485-97.

[17] McCormick PG, Liu Y. Thermodynamic analysis of the martensitic transformation in NiTi-II. Effect of transformation cycling. Acta Metall Mater 1994; 42:2407-13.

[18] Pelton AR, Huang GH, Moine P, Sinclair R. Effects of thermal cycling on microstructure and properties in Nitinol. Mater Sci Eng A 2012; 532:130-38.

[19] Wang ZG, Zu XT, Huo Y. Effect of heating/cooling rate on the transformation temperature in TiNiCu shape memory alloys. Thermochim Acta 2005; 436:153-5.

[20] Nurveren K, Akdogan A, Huang WM. Evolution of transformation characteristics with heating/cooling rate in NiTi shape memory alloys. J Mater Process Technol 2008;196:129-34.

[21] Kissinger HE. Reaction kinetics in differential thermal analysis. Anal Chem 1957; 29:1702-6.

[22] Inaekyan K, Brailovski V, Prokoshkin S, Korotitskiy A, Glezer A. Characterization of amorphous and nanocrystalline Ti-Ni-based shape memory alloys. J Alloys Compd 2009; 473:71-8.

[23] Ozgen S, Tatar C. Thermoelastic transition kinetics of a gamma irradiated CuZnAl shape memory alloy. Met Mater Int 2012; 18: 909-16.

[24] Canbay CK, Aydogdu A, Aydogdu Y. The investigation of thermal and magnetic properties and microstructure analysis of Cu-Al-Mn shape memory alloys. J Supercond Nov Magn 2011;24:871-7.

[25] Ramaiah KV, Saikrishna CN, Bhagyaraj J, Gouthama, Bhaumik SK. Influence of Sc addition on microstructure and transformation behaviour of $Ni_{24.7}Ti_{50.3}Pd_{25.0}$ high temperature shape memory alloy. Intermetallics 2013; 40:10-18.

[26] Rajagopalan S, Little AL, Bourke MAM, Vaidyanathan R. Elastic modulus of B19' shape memory NiTi from in situ neutron diffraction during loading, instrumented nanoindentation and extensometry. Appl Phys Lett 2005; 86: 081901-03.

[27] Sinha A, Chattopadhyay PP. Nanomechanical response of martensite in Ti-(~49at.%) Ni alloy. Mater Sci. Eng. A 2012; 552:540-6.

[28] Mei QS, Zhang L, Tsuchiya K, Gao H, Ohmura T, Tsuzaki K. Grain size dependence of the elastic modulus in nanostructured NiTi. Scripta Mater 2010; 63:977-80.

[29] Yang B, Riester L, Nieh TG. Strain hardening and recovery in a bulk metallic glass under nanoindentation. Scripta Mater 2006; 54: 1277-80.

[30] Gall K, Maier HJ. Cyclic deformation mechanisms in precipitated NiTi shape memory alloys. Acta Mater 2002; 50:4643-57.

[31] Hamilton RF, Sehitoglu H, Chumlyakov Y, Maier HJ. Stress dependence of the hysteresis in single crystal NiTi alloys. Acta Mater 2004; 52:3383-402.

[32] Ortin J, Planes A. Thermodynamic analysis of thermal measurements in thermoelastic martensitic transformations. Acta Metall 1988; 36:1873-89.

[33] Dirand L, No ML, Chastaing K, Denquin A, Juan JS. Internal friction and dynamic modulus in Ru-50Nb ultra-high temperature shape memory alloys. Appl Phys Lett 2012; 101:161909-12.

[34] Chang SH, Wu S. Inherent internal friction of $Ti_{51}Ni_{39}Cu_{10}$ shape memory alloy. Mater Trans JIM 2007; 48:2143-7.

[35] Salzbrenner RJ, Cohen M. On the thermodynamics of thermoelastic martensitic transformations. Acta Metall 1979; 27:739-48.

[36] Grossmann CH, Frenzel J, Sampath V, Depka T, Eggeler G. Elementary transformation and deformation processes and the cyclic stability of NiTi and NiTiCu shape memory spring actuators. Metall Mater Trans A 2009; 40:2530-44.

[37] Matsuda M, Hara T, Nishida M. Crystallography and morphology of antiphase boundary-like structure induced by martensitic transformation in Ti-Pd shape memory alloy. Mater Trans JIM 2008; 49:461-5.

[38] Matsuda M, Kuramoto K, Morizono Y, Tsurekawa S, Okunishi E, Hara T, Nishida M. Transmission electron microscopy of antiphase boundary-like structure of B19′ martensite in Ti-Ni shape memory alloy. Acta Mater 2011;59:133-40.

[39] Ball JM, James RD. Proposed experimental tests of a theory of fine microstructure and the two-well problem. Philos Trans R Soc Lond A 1992; 338:389-450.